Wide-field adaptive optics performance in cosmological deep fields for multi-object spectroscopy with the European Extremely Large Telescope

A. G. Basden,[1]⋆ C. J. Evans[2] and T. J. Morris[1]

[1]*Department of Physics, South Road, Durham DH1 3LE, UK*

[2]*UKATC, Royal Observatory, Blackford Hill, Edinburgh EH9 3HJ, UK*

ABSTRACT

A multi-object spectrograph on the forthcoming European Extremely Large Telescope will be required to operate with good sky coverage. Many of the interesting deep cosmological fields were deliberately chosen to be free of bright foreground stars, and therefore are potentially challenging for adaptive optics (AO) systems. Here, we investigate multi-object AO performance using subfields chosen at random from within the Great Observatories Origins Deep Survey (GOODS)-S field, which is the worst case scenario for five deep fields used extensively in studies of high-redshift galaxies. Our AO system model is based on that of the proposed MOSAIC instrument but our findings are equally applicable to plans for multi-object spectroscopy on any of the planned Extremely Large Telescopes. Potential guide stars within these subfields are identified and used for simulations of AO correction. We achieve ensquared energies within 75 mas of between 25–35 per cent depending on the subfield, which is sufficient to probe sub-kpc scales in high-redshift galaxies. We also investigate the effect of detector readout noise on AO system performance, and consider cases where natural guide stars are used for both high-order and tip-tilt-only AO correction. We also consider how performance scales with ensquared energy box size. In summary, the expected AO performance is sufficient for a MOSAIC-like instrument, even within deep fields characterized by a lack of bright foreground stars.

Key words: instrumentation: adaptive optics – instrumentation: high angular resolution – methods: numerical.

1 INTRODUCTION

One of the primary scientific motivations for the forthcoming Extremely Large Telescopes (ELTs), which will have primary mirror diameters in excess of 20 m, is to understand the evolution of galaxies – from formation of the most distant systems known, seen only a few million years after the big bang, through to disentangling the structural components and histories of the nearby galaxies that we see today.

Many of the breakthroughs in galaxy studies over the past 20 yr have been enabled by observations of selected 'deep fields' on the sky. The core data sets for these efforts have been optical and near-infrared imaging from long integrations with the *Hubble Space Telescope*(*HST*) and ground-based observatories, complemented by a wealth of multiwavelength information from facilities such as *Chandra*, *Spitzer*, *Herschel* and the Very Large Array (VLA).

Given the substantial observational investment in these fields, and the richness of the multiwavelength data available, they will

almost certainly be the target of future programmes with both the *James Webb Space Telescope* (*JWST*; Gardner et al. 2006) and the European ELT (E-ELT; Spyromilio et al. 2008). Specifically, many of the sources known in these fields are sufficiently faint that they are beyond our current spectroscopic capabilities, and follow-up spectroscopy will require the improved sensitivities of these exciting new facilities.

One of the most important new techniques for studies of high-redshift galaxies over the past decade has been the development of integral-field spectrographs (IFSs) on 8–10 m class telescopes. These have enabled *spatially resolved* studies of galaxies out to a redshift of $z \sim 3$ (see e.g. the review by Glazebrook 2013). In particular, the use of adaptive optics (AO) with IFS instruments has provided unprecedented views of the substructure and physical properties of high-z galaxies (see e.g. the comparisons of AO-corrected and seeing-limited observations from Newman et al. 2013).

However, at $z \gtrsim 1.5$ we are currently limited to spatially resolved spectroscopy of only the most luminous and/or massive galaxies; to observe a representative sample of the galaxy population in the early Universe we require the spectroscopic sensitivity of the European ELT (E-ELT). Moreover, to compile large samples (of thousands) of

⋆ E-mail: a.g.basden@durham.ac.uk

objects within a realistic observing time, we require the combination of multiple integral field units (IFUs) and a wide-field AO system.

The technical requirements for such observations, in particular the necessary AO performances, were presented by Puech et al. (2008, 2010). In brief, to probe scales of ∼1 kpc at high redshift (e.g. Bournaud, Elmegreen & Elmegreen 2007), we require ensquared energies of 20–30 per cent in ∼75 mas in the *H* band. Coarser sampling of ∼100–150 mas (with comparable ensquared energy) is sufficient for the recovery of large-scale dynamics in the target galaxies. These requirements strongly influenced the conceptual design for the proposed EAGLE instrument (Cuby et al. 2010), and they are now shaping the design of the MOSAIC concept (Evans et al. 2014; Hammer et al. 2014) for a multi-object spectrograph (MOS) for the E-ELT. As noted above, many of the potential targets for MOS observations with any of the planned ELTs will likely be located in the existing extragalactic deep fields. To achieve the multi-object AO (MOAO) correction for an instrument such as MOSAIC, we need natural guide stars (NGSs) within the patrol field of the instrument, but a key feature of the deep fields was that they were deliberately chosen to be free of relatively bright foreground stars (to avoid problems relating to saturation, diffraction, persistence, etc.). For example, the lack of suitable guide stars ($V < 14$) within a 2 arcmin × 2 arcmin field for observations with the Multi-Conjugate Adaptive Optics Demonstrator (MAD; Marchetti et al. 2007), severely limited its use to observe cosmological deep fields.

In the following, we therefore investigate whether we can obtain sufficient image quality for spatially resolved spectroscopy of high-z galaxies in one of the most important extragalactic deep fields, the Great Observatories Origins Deep Survey (GOODS)-S field (Giavalisco et al. 2004). The GOODS-S field is one of five observed as part of the Cosmic Assembly Near-infrared Deep Extragalactic Legacy Survey (CANDELS; Grogin et al. 2011; Koekemoer et al. 2011), providing unprecedented depth and wavelength coverage for such a large area of *HST* imaging. In addition to the rich photometric catalogues, there has been significant spectroscopic follow-up of galaxies in the GOODS-S field (e.g. Popesso et al. 2009), and this will be extended by the recently approved VANDELS ESO Public Spectroscopic Survey (PIs: R. McLure & L. Pentericci). Thus, in the coming years we will have considerable information in the GOODS-S region to select well-defined samples of target galaxies for spatially resolved spectroscopy with the ELTs.

In addition to considering the GOODS-S field, we have performed a study of other fields including GOODS-N, UDS, EGS and COSMOS (Grogin et al. 2011). Within each of these fields, we have taken a random sample of ten 10 arcmin subfields and determined the number of stars within these fields with an r' magnitude of brighter than 16, and thus available for high-order wavefront sensing (i.e. delivering more than a few photons per subaperture per frame). Table 1 shows the number of suitable NGSs within these subfields; the GOODS-S field provides the fewest guide stars within its subfields. We have therefore chosen these subfields for further study as the pessimistic case: our results are equally applicable for the other fields.

The NFIRAOS system on the Thirty Metre Telescope (TMT) has a science goal of 50 per cent sky coverage, and is expected to deliver AO correction over most of the observable sky for 50 per cent of fields (Andersen et al. 2011). The increased light collecting area of the E-ELT will further improve field observability. Since the GOODS-S field is looking directly out of the Milky Way galaxy, it is a pessimistic case. Indeed, a statistical approach to sky coverage for the E-ELT by European Southern Observatory (ESO; Calamida 2009) found that, in a typical field at the latitude of the GOODS-S

Table 1. NGS availability within 10 random 10 arcmin subfields from within the given cosmological deep fields. The numbers presented are the number of subfields containing only N NGSs with $r' < 16$ mag.

Field	Subfields containing only N guide stars								
	$N = 2$	3	4	5	6	7	8	9	>9
GOODS-S	1	2	2	4	1	0	0	0	0
GOODS-N	0	1	2	1	2	2	1	1	0
UDS	0	0	0	0	0	2	3	3	2
EGS	0	1	0	0	2	1	2	1	3
COSMOS	0	0	0	0	0	0	0	0	10

field, we would expect more guide stars than we find in this field (it is pessimistic), and that even at the Galactic pole we would expect at least a couple of stars. Therefore, we are confident that the fields under consideration here are relevant for the whole sky.

In Section 2, we introduce the NGS fields that we investigate, and provide details of the AO modelling that we perform. In Section 3, we discuss our results, and we conclude in Section 4.

2 MODELLING OF ELT AO IN THE GOODS-S FIELD

Within the GOODS-S Deep + Wide + ERS survey region from CANDELS we generated 10 random 10 arcmin diameter fields to investigate potential NGS asterisms. Using the data assembled for the fourth United States Naval Observatory CCD Astrograph Catalog (UCAC4; Zacharias et al. 2013), we recovered the positions and magnitudes of stars within each field (which are complete down to $R \sim 16$ mag), and used these as inputs to investigate the range of simulated AO performances. Specifically, we use the cross-matched Sloan r'-band magnitudes (in the AB system) from the American Association of Variable Star Observers (AAVSO) Photometric All-Sky Survey (APASS).

Fig. 1 shows the fields that we have investigated, giving the NGSs available within these fields and their corresponding r'-band magnitudes. For reference, we also show the notional laser guide star (LGS) positions. The field centres are given in Table 2, and the overlap of the fields is shown graphically in Fig. 2. A key point of this study is that of random field selection, and by estimating AO performance in randomly selected subfields, we are able to demonstrate the availability of suitable NGS targets over the whole of the GOODS-S field. The alternative approach would be to determine all the NGS asterisms providing good AO performance within the GOODS-S field. However, it would then be necessary to accept that, if a scientific target lay just outside the corrected field of view, it would not be observable, or at least, the AO correction would be lower than required.

The faintest target that we consider has an r' magnitude of 16.3, which we translate to about three detected photons per subaperture per frame. We do not consider the use of any fainter targets as too few photons would be received. In the cases where NGSs are used for tip-tilt correction only, it would be possible to further reduce the source flux, though we do not investigate this here since the lack of high-order NGS information then leads to reduced AO performance (even if the tip-tilt stars are very bright).

2.1 AO simulations

We use a Monte Carlo simulation tool (Basden et al. 2007), the Durham AO simulation platform (DASP), to provide performance
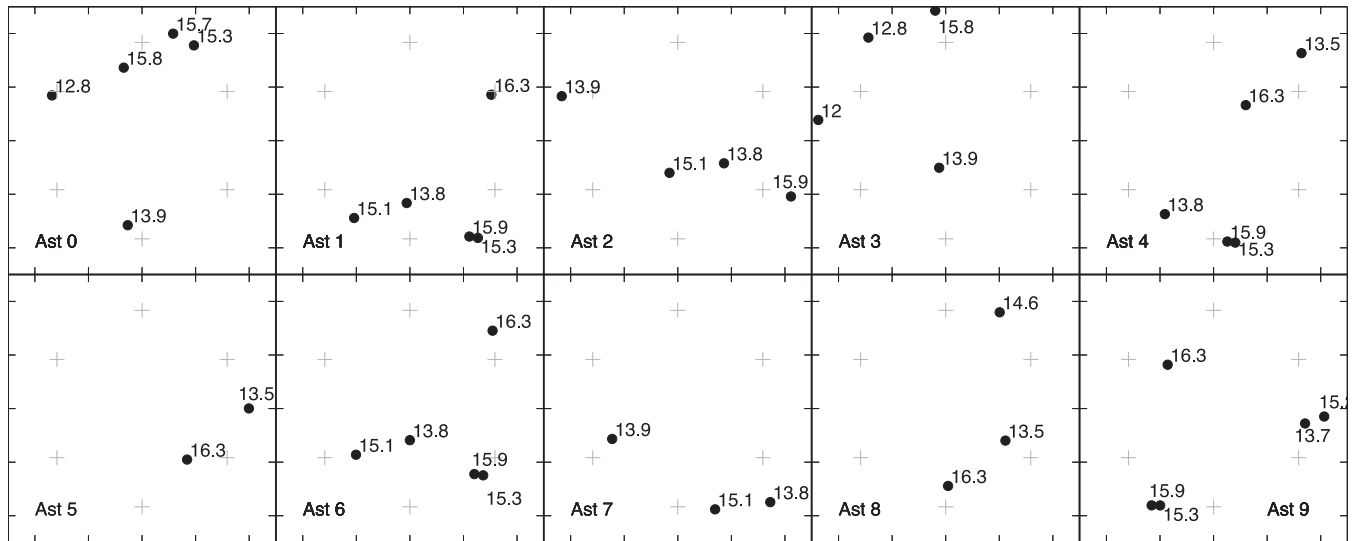
Figure 1. The 10 NGS asterisms used to investigate potential AO performance in the GOODS-S field. Each subfield is 10 arcmin in diameter. The numbers within these figures provide the corresponding guide star r'-band magnitudes, and the grey crosses show LGS positions.

Table 2. Central coordinates for the 10 arcmin fields in which we have investigated the AO performances (J2000).

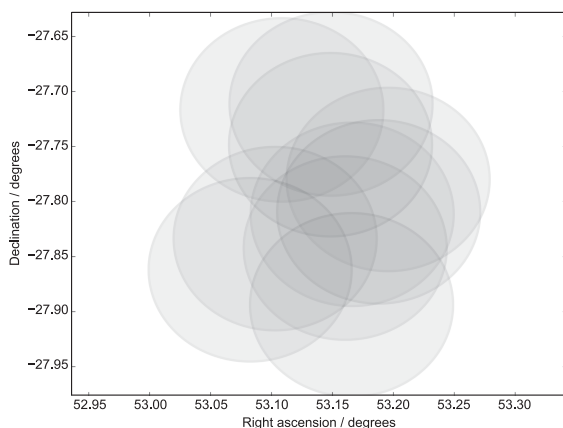| Asterism	RA / degrees	Dec. / degrees
0	53.108 505 25	−27.716 682 43
1	53.166 233 06	−27.811 525 34
2	53.195 743 56	−27.779 848 10
3	53.148 849 49	−27.711 238 86
4	53.160 507 20	−27.842 172 62
5	53.102 977 75	−27.833 610 53
6	53.187 988 28	−27.809 297 56
7	53.148 445 13	−27.748 273 85
8	53.082 466 13	−27.861 900 33
9	53.165 714 26	−27.893 751 14

Figure 2. Positions of the 10 random fields used to investigate potential NGS asterisms, within the GOODS-S field. The circles represent the 10 arcmin field of view of the telescope at each location.

estimates for a MOAO-corrected MOS on the E-ELT, using the NGS asterisms defined in Fig. 1. The model has the same basic form as that used for performance modelling of the EAGLE concept (Basden, Myers & Butterley 2010), and previous analysis of

E-ELT MOAO performances (Basden et al. 2013; Basden 2014). Although the exact details of the MOSAIC concept are still under study (e.g. number and final specification of science channels), our objective here was to investigate the broader aspects of a MOAO-corrected MOS, so we investigate a wide range of NGS magnitudes (Section 3), detector performances (Section 3.1), tip-tilt correction (Section 3.2) and spatial element size on the sky (Section 3.3). We note that the MOAO performance across the telescope field of view has been investigated previously (Basden et al. 2013), so here we provide on-axis performance estimates (at the centre of the LGS asterism) to simplify our results.

In summary, we use six sodium LGSs (589 nm wavelength) equally spaced around the edge of a 7.3 arcmin diameter circle (the widest LGS asterism that can be transported to the E-ELT focal plane), each with 74×74 subapertures and 16×16 pixels per subaperture. The telescope diameter is taken to be 38.5 m, and has a pupil function taken to match that of the multihexagon E-ELT. The secondary mirror obscuration is about 11 m in diameter, and the deformable mirror (DM) pitch is 52 cm. We have used a set of 35 layer atmospheric profiles, available on request from the European Southern Observatory (ESO). This profile is the result of years of data collection at the Paranal Observatory, and has an outer scale of $L_0 = 25$ m, and a Fried's parameter of $r_0 = 15.7$ cm defined at zenith. In the simulations presented here, we assume that observations are made at $30°$ from zenith. We include the cone effect (due to the finite distance to the LGS spots) and spot elongation, assuming a sodium-layer profile with a Gaussian shape centred at 90 km with a 5 km full width at half-maximum (FWHM). We use up to five NGSs, depending upon availability, and these are also sampled by 74×74 Shack–Hartmann wavefront sensor subapertures, which operate at the centre of the r' band (625 nm). We do not take NGS chromatic effects into consideration. We include photon shot noise in our wavefront sensors (WFSs), and our default case includes no readout noise, though we investigate the effect on performance that this has in Section 3.1. In recent years, both electron multiplying CCD (EMCCD) and scientific CMOS (sCMOS) technologies have progressed significantly, and so it is likely that very low readout noise levels will be achievable within the time frame of ELT instrumentation. EMCCDs (Basden, Haniff & Mackay 2003)

routinely achieve 0.1 photoelectrons readout noise (with further reductions possible depending on their mode of operation), and sCMOS technology now achieves levels as low as 0.9 photoelectrons. For simplicity, we use a basic centre-of-gravity algorithm to estimate wavefront slope for both LGS and NGS WFSs, even though it has previously been shown that other algorithms can yield better performance, for example using correlation methods (Basden et al. 2014).

The E-ELT M4 DM is assumed to be conjugated to the ground-layer turbulence, and has 75×75 actuators. We investigate the *H* band on-axis performance and use a MOAO DM with 75×75 actuators. Unless otherwise stated, our primary performance metric is the percentage of the point spread function (PSF) ensquared energy within 75 mas, chosen to match the scales of interest in high-*z* galaxies (Puech et al. 2008). A tomographic reconstruction of the atmospheric turbulence is performed using a minimum variance formulation, with phase covariance approximated by a Laplacian function. Noise covariance is assumed to be constant for each WFS, and dependent on guide star signal level. Wavefront reconstruction involves a virtual DM formulation, and we use 12 virtual DMs, having found that there is insignificant performance gain when additional DMs (with associated increased simulation complexity) are introduced with the 35 layer atmosphere model. The reconstructed phase is then projected on to the physical DMs, which perform the AO correction. We model DMs using an interpolated spline function, which gives a good fit to surface models of most known DM types.

We assume an AO system update rate of 250 Hz, a baseline for MOSAIC, since the MOAO DMs will be operated in open-loop, and simulate 20 s of telescope time, verifying that the PSFs have converged. We note that the CANARY MOAO demonstration instrument (Myers et al. 2008) can also be operated at 250 Hz.

A previous study has shown that AO correction for the LGS configuration considered here is relatively constant over the field of view, differing by only a few per cent in ensquared energy (Basden et al. 2013). Here, we therefore concentrate on the on-axis direction which is furthest from the LGS locations.

2.1.1 Guide star signal level

We base our NGS signal levels on r′ magnitudes, centred at $\lambda = 625$ nm with a $\delta\lambda = 140$ nm bandwidth (Fukugita et al. 1996). At magnitude 0, the r′ band gives a flux, *F* of 3631 Jy (Oke & Gunn 1983), and therefore a zero-magnitude star gives 1.23×10^{10} photons m^{-2} s^{-1}. We assume a telescope throughput of $T_{\text{tel}} = 90$ per cent (see e.g. Puech et al. 2010), and a WFS throughput of $T_{\text{wfs}} = 85$ per cent, giving a final flux estimation equal to

$$s = F \times J \times 10^{-0.4r'} \frac{A}{f} \times T_{\text{tel}} \times T_{\text{wfs}}, \qquad (1)$$

where *s* is the NGS signal in photons per subaperture per frame, and r′ is the guide-star magnitude. $J = 1.51 \times 10^7$ photons per second per square metre per fractional bandwidth ($\frac{\delta\lambda}{\lambda}$). *A* is the subaperture area, 0.5^2 m^2, and *f* is the AO frame rate of 250 Hz.

Because there are many uncertainties in this flux calculation, we also investigate simulation performance as a function of a scaling of this signal level, allowing estimates to be updated once factors such as actual guide star observation band (and bandwidth, since WFSs can be very broad-band with appropriate atmospheric dispersion correction) and detector quantum efficiency are known.

It should be noted that these signal levels are very faint. The faintest star in the NGS asterisms that we investigate has an r′

magnitude of 16.3, giving about three photons per subaperture per frame, according to equation (1). We take no special measures with such faint guide stars: they are processed in the same way as all others. However, because we use a maximum a priori wavefront reconstruction algorithm, WFS noise is taken into consideration, and signals from noisier WFs are penalized. Guide star signal levels could be increased by reducing the WFS frame rate. However, we do not consider this option here, partly because we are unable to easily operate LGS and NGS WFSs at different rates in our simulations, and because the improvement in performance would only be slight, for a large gain in complexity: we already take WFS noise into consideration in our wavefront reconstruction, and because the correction of the high spatial frequencies using high-order WFSs requires high time resolution, with reducing effectiveness as frame rate decreases. However, it should be noted that a reduction in NGS frame rate is likely to lead to a small improvement in AO performance when the faintest NGSs are considered.

We assume that LGS signal levels are not photon-limited (Holzlöhner et al. 2010).

3 MOAO PERFORMANCE IN THE GOODS-S FIELD

Evaluating the AO performance for each asterism at the reference signal level alone will only give a performance snapshot for this signal level. We therefore consider increasing and reducing the signal levels across the board (i.e. for all NGS), for each asterism under consideration. Fig. 3 shows that the signal levels available for guide stars within the GOODS-S field are indeed low, and that an order of magnitude increase in flux (2.5 astronomical magnitudes) is required to ensure that there is then little performance gain by further increasing the signal levels. However, it also shows that at the reference flux levels, between 25–35 per cent ensquared energy within 75 mas can be achieved (this increases to 30–38 per cent when flux is not the limiting factor). The uncertainties within the model (based on repeat simulations) for this, and the following, figures are at the 1 per cent level (not shown in the figures to aid clarity).

Fig. 4 shows the AO corrected PSF FWHM as a function of signal level, compared with the theoretical diffraction limit for a 38.5 m
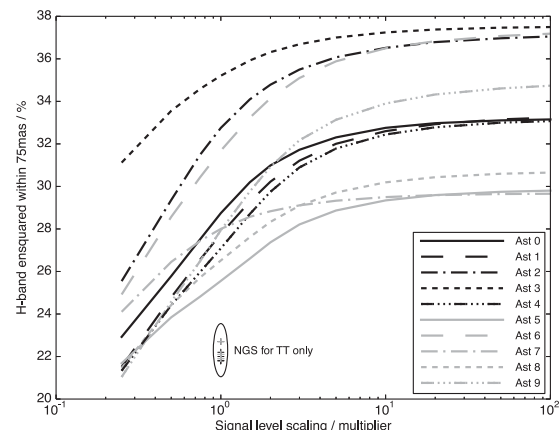
Figure 3. AO performance (ensquared energy) as a function of NGS asterism signal level scaling (with all guide star signals scaled by the *X*-axis value). For reference, the range of performance achieved when NGS information is used for tip-tilt correction only is also shown, and gives constant AO performance between signal level scales from 1 to 100. The legend provides the asterism number (ast).
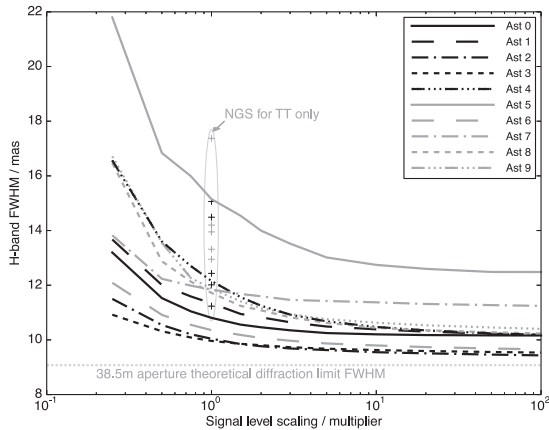
Figure 4. AO performance (FWHM) as a function of NGS asterism signal level scale (with all guide star signals scaled by the *X*-axis value). For reference, the range of performance achieved when NGS information is used for tip-tilt correction only is also shown, and gives constant AO performance between signal level scales from 1 to 100. The theoretical aperture limit is also shown, corresponding to the FWHM of a diffraction-limited spot on a 38.5 m aperture.

aperture. For the unmodified signal level (a scaling factor of unity), all asterisms lead to a PSF with an FWHM less than twice that of the theoretical, with some being only 10 per cent larger. The PSFs themselves are shown in Fig. 5 for the case of default signal level. All the PSFs are well constrained, however, in the case of asterism 5, significant structure is displayed due to the presence of only two guide stars (one of which being very faint).

3.1 The effect of readout noise on AO performance

We have so far assumed that our detectors have no readout noise, with photon shot noise being the only WFS noise source. We now consider the AO performance when NGS readout noise is introduced. We have considered readout noise levels based on current detector technologies, ranging from 0.01 photoelectrons to 1 photoelectron. Fig. 6 shows the AO performance as a function of readout noise for the different NGS asterisms under consideration. Here, we can see that noise can have a significant effect on performance, and therefore careful consideration should be given to the detector technology (EMCCD or sCMOS) used.

We have not considered detector quantum efficiency or the excess noise factor introduced by EMCCDs (which can effectively halve the quantum efficiency), though the effect that this has on performance can be garnered from Fig. 3: it can be seen that with a signal level scaling of 0.5 (due to the EMCCD excess noise factor), the AO performance is higher than that with a readout noise of 1
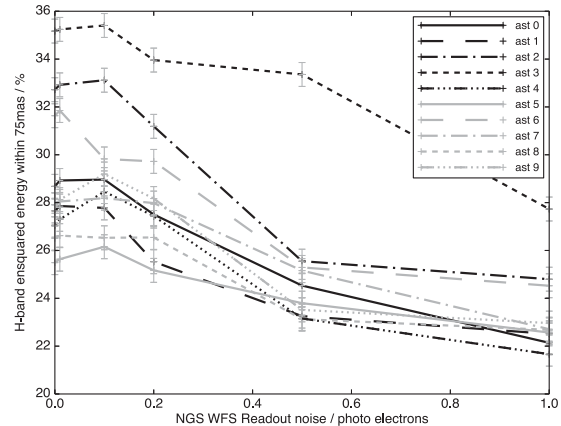

Figure 6. AO performance as a function of NGS readout noise, for the different asterisms under consideration here.

photoelectron in Fig. 6 (corresponding to an sCMOS detector). This suggests that EMCCD technology is more appropriate here.

Detector readout noise is key to the AO performance. However, our treatment of the effect of noise has been basic: we have simply removed a background level after adding readout noise (with a random Gaussian distribution) and relied on the minimum variance wavefront reconstruction. We have ignored sky background, which is low in the *r'* band at 250 Hz frame rates. We have not considered more advanced techniques often employed in AO, for example pixel calibration based on brightest pixels within a subaperture (Basden, Myers & Gendron 2012), or Gaussian noise removal algorithms. The baseline for the EAGLE concept (Cuby et al. 2008), a forerunner for MOSAIC, was to use Shack–Hartmann WFs, and we have therefore not considered other sensor types. We have also not considered the benefits that could be obtained by reducing the number of NGS subapertures. Further, we have not considered the change in performance if the faintest stars within an asterism are disregarded (i.e. not used for AO), which may reduce noise propagation and hence increase AO performance. Therefore, it is likely that performance improvements could be realized when using noisy detectors over the results presented here, which can therefore be taken as pessimistic. The upper bound to performance, however, is given by the high flux cases in Fig. 3.

3.2 NGS for tip-tilt correction only

Given that the NGS signal levels are very low for many of the guide stars available within the selected GOODS-S subfields, it is worth considering the AO performance obtained when the NGS are used for tip-tilt correction only. Even using the faintest guide stars
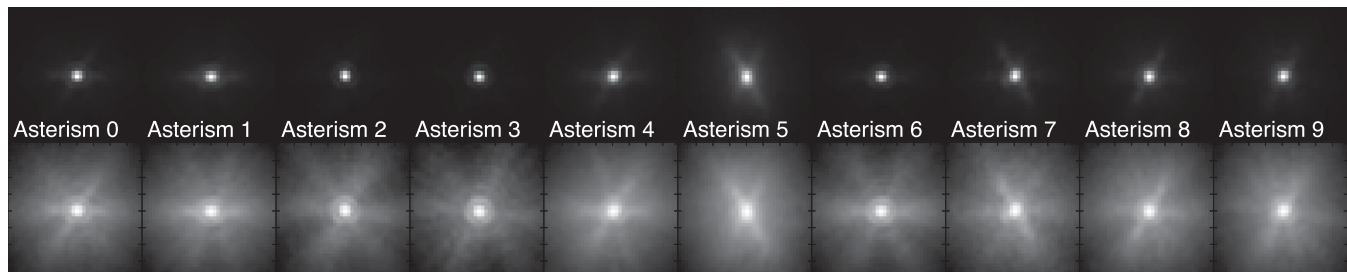

Figure 5. Simulated AO corrected *H*-band PSFs for the 10 asterisms under consideration here. Each PSF box has an edge size of 177 mas. The top row shows the PSF, while the bottom row shows the natural logarithm of the PSF, showing the underlying hexagonal structure due to the LGS arrangement.

available provides ample signal for tip-tilt estimation, with thousands of photons collected across the telescope aperture. However, this then results in a lack of tomographic wavefront information, since the wide LGS asterism is unable to fully sample the turbulent volume. We find that the AO performance is reduced to about 22–23 per cent ensquared energy within 75 mas, irrespective of the NGS asterism used (Fig. 3). NGS tip-tilt-only correction within the GOODS-S field is therefore not optimal: the high-order information obtainable from the NGSs is valuable. We also find that there is no increase in performance when guide star flux is increased by up to a factor of 100 beyond the nominal flux (levelling off at about 10 times flux, i.e. NGSs which are 2.5 magnitudes brighter than those studied here).

3.3 Ensquared energy diameter

The fractional ensquared energy as a function of spatial size on the sky is shown in Fig. 7. We have shown the best and worst asterisms in terms of performance (asterisms 5 and 7, respectively), and provide results for the default case, for an increase in the NGS signal by a factor of 10 (where the AO performance approaches that of the high light-level case), and for when no high-order NGS information is used (i.e. the NGS are only used to determine the required tip-tilt correction). These results will directly inform design decisions for the MOSAIC concept, and their trends will be relevant to discussions of IFU spaxel size verses expected performance for other future instruments.

We have selected our primary performance criterion to be the ensquared energy of the PSF within 75 mas, as motivated by the science simulations from Puech et al. (2008), with an updated discussion of these issues given by Evans et al. (2013). This spatial scale (sampled by two IFU spaxels) was the baseline for the EAGLE concept, and represents the most demanding requirement on spatial resolution in recent studies of a MOAO-corrected MOS. As noted in Section 1, slightly coarser sampling of 100–150 mas (i.e. spatial pixels of 50–75 mas), with comparable ensquared energy, is sufficient to recover the global properties of high-z galaxies. Such a spaxel size is also a good match for spectroscopic follow-up of resolved stellar populations observed with the *HST* and, in the future, the *JWST* (see discussion by Evans et al. 2013).
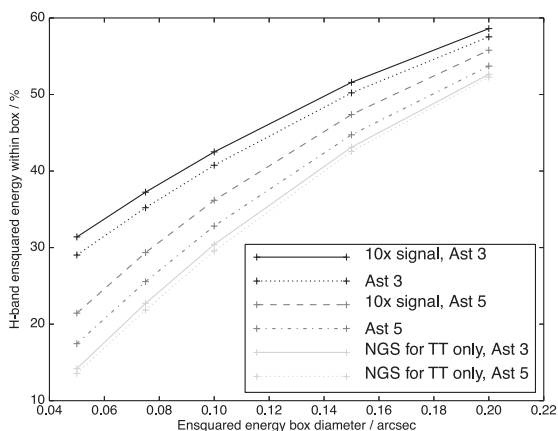

Figure 7. The fraction of PSF energy ensquared as a function of box size. As shown in the legend, results are for the best (3) and worse (5) performing NGS asterisms, for three separate cases: when the NGS signal level is increased by a factor of 10, for the default NGS signal level and for the case where NGS information is only used for tip-tilt correction.

The top-level requirements for MOSAIC demand spaxel sizes which range from 40 to ∼100 mas (see table 3 from Evans et al. 2014). Compared to the ensquared energy requirements from Puech et al. (2008), the 25–35 per cent ensquared energy in 75 mas from the simulated fields in this work satisfy the most demanding requirements. Relaxing the spatial scales slightly (to, for example, the ensquared energy within 150 mas) leads to an ensquared energy estimate of 40–50 per cent (Fig. 7). This would provide more than enough scope for additional reductions in performance from effects not modelled here (e.g. wavefront errors in the instrument could potentially degrade the ensquared energy by ∼10 per cent, e.g. Laporte, Schnetler & Rousset (2010), while also satisfying the requirements for the vast majority of the science cases from Evans et al. (2013, 2014).

3.4 Future work

We have not considered techniques which make optimum use of NGS signals, rather relying on the minimum variance wavefront reconstruction with WFS noise covariance approximations. However, other approaches are also possible, which we intend to investigate. This includes the use of multirate WFSs, allowing lower frame rates for NGS observing faint targets, and a reduction of WFS order. Both techniques would increase the number of detected photons per subaperture per frame, and would therefore lead to more accurate wavefront slope estimation.

4 CONCLUSIONS

We have investigated the performance of an ELT MOAO instrument, giving consideration to the effect of NGS availability on performance. We have selected an existing deep cosmological field, the GOODS-S field, for this study, which is one of five fields observed as part of the *HST* CANDELS survey, providing rich scientific potential for ELT spectroscopy. 10 subfields within this region were chosen at random, and the expected AO performance investigated. Within each subfield, we found at least two sufficiently bright NGSs, even though a key feature of the deep fields is that they are deliberately free of bright stars ($V < 14$). We have investigated the AO performance as a function of flux from these guide stars, to allow for uncertainties in detector efficiency and telescope optical throughput.

We find it is beneficial to use high-order wavefront information from faint NGSs as opposed to tip-tilt information. This conclusion should be revisited once the magnitude of additional tip-tilt components present within the system (e.g. from telescope vibrations) are better characterized.

Our key AO performance metric is the ensquared energy within 75 mas, which is between 25–35 per cent for all of the NGS asterisms considered, reducing to about 22 per cent when no high-order NGS information is used. An increase in ensquared energy to 40–50 per cent is possible with a box size of 150 mas. The AO performance that we predict here is sufficient for the proposed MOSAIC instrument.

REFERENCES

Andersen D., Wang L., Ellerbroek B., Herriot G., 2011, in 2nd Int. Conf. on Adaptive Optics for Extremely Large Telescopes. Observatoire de Paris, Paris, p. 18P

Basden A. G., 2014, MNRAS, 440, 577

Basden A. G., Haniff C. A., Mackay C. D., 2003, MNRAS, 345, 985

Basden A. G., Butterley T., Myers R. M., Wilson R. W., 2007, Appl. Opt., 46, 1089

Basden A., Myers R., Butterley T., 2010, Appl. Opt., 49, G1

Basden A. G., Myers R. M., Gendron E., 2012, MNRAS, 419, 1628

Basden A. G., Bharmal N. A., Myers R. M., Morris S. L., Morris T. J., 2013, MNRAS, 435, 992

Basden A. G., Chemla F., Dipper N., Gendron E., Henry D., Morris T., Rousset G., Vidal F., 2014, MNRAS, 439, 968

Bournaud F., Elmegreen B. G., Elmegreen D. M., 2007, ApJ, 670, 237

Calamida A., 2009, Technical Report E-TRE-ESO-0800588 issue 1, Stellar Counts for the E-ELT Sky Coverage. ESO, Garching

Cuby J.-G. et al., 2008, in McLean I. S., Casali M. M., eds, Proc SPIE Conf. Ser. Vol. 7014, Ground-based and Airborne Instrumentation for Astronomy II. SPIE, Bellingham, p. 70141K

Cuby J.-G. et al., 2010, in McLean I S., Ramsay S. K., Takami H., eds, Proc SPIE Conf. Ser. Vol. 7735, Ground-based and Airborne Instrumentation for Astronomy III. SPIE, Bellingham, p. 77352D

Evans C. et al., 2013, in Evans C., ed, Tech. Rep., UK-ATC, ELT-MOS White Paper: Science Overview and Requirements. UK Astronomy Technology Centre, Edinburgh

Evans C. J. et al., 2014, Proc. SPIE, 9147, 914796

Fukugita M., Ichikawa T., Gunn J. E., Doi M., Shimasaku K., Schneider D. P., 1996, AJ, 111, 1748

Gardner J. et al., 2006, Space Sci. Rev., 123, 485

Giavalisco M., Ferguson H. C., Koekemoer A. M., Dickinson M., Alexander D. M., Bauer F. E., Bergeron J., 2004, ApJ, 600, L93

Glazebrook K., 2013, PASA, 30, 56

Grogin N. A., Kocevski D. D., Faber S. M., Ferguson H. C., Koekemoer A. M., Riess A. G., Acquaviva V., 2011, ApJS, 197, 35

Hammer F. et al., 2014, Proc. SPIE, 9147, 914727

Holzlöhner R., Rochester S. M., Pfrommer T., Bonaccini Calia D., Budker D., Higbie J. M., Hackenberg W., 2010, in Ellerbroek B. L., Hart M., Hubin N., Wizinowich P. L., eds, Proc SPIE Conf. Ser. Vol. 7736, Adaptive Optics Systems II. SPIE, Bellingham, p. 77360V

Koekemoer A. M. et al., 2011, ApJS, 197, 36

Laporte P., Schnetler H., Rousset G., 2010, in Angeli G. Z., Dierickx P., eds, Proc SPIE Conf. Ser. Vol. 7738, Modeling, Systems Engineering, and Project Management for Astronomy IV. SPIE, Bellingham, p. 77381B

Marchetti E. et al., 2007, The Messenger, 129, 8

Myers R. M. et al., 2008, in Hubin N., Max C. E., Wizinowich P. L., eds, Proc SPIE Conf. Ser. Vol. 7015, Adaptive Optics Systems. SPIE, Bellingham, p. 70150E

Newman S. F., Genzel R., Forster Schreiber N. M., Shapiro Griffin K., Mancini C., Lilly S. J., Renzini A., 2013, ApJ, 767, 104

Oke J. B., Gunn J. E., 1983, ApJ, 266, 713

Popesso P. et al., 2009, A&A, 494, 443

Puech M., Flores H., Lehnert M., Neichel B., Fusco T., Rosati P., Cuby J.-G., Rousset G., 2008, MNRAS, 390, 1089

Puech M., Rosati P., Toft S., Cimatti A., Neichel B., Fusco T., 2010, MNRAS, 402, 903

Spyromilio J., Comerón F., D'Odorico S., Kissler-Patig M., Gilmozzi R., 2008, The Messenger, 133, 2

Zacharias N., Finch C. T., Girard T. M., Henden A., Bartlett J. L., Monet D. G., Zacharias M. I., 2013, AJ, 145, 44

This paper has been typeset from a TₑX/LATₑX file prepared by the author.